npj | Quantum Materials

www.nature.com/npjquantmats

ARTICLE OPEN

Excitations in the field-induced quantum spin liquid state of α-$RuCl_3$

Arnab Banerjee[1,2], Paula Lampen-Kelley[3,4], Johannes Knolle[5], Christian Balz[1,2], Adam Anthony Aczel[1,2], Barry Winn[1,2], Yaohua Liu[1,2], Daniel Pajerowski[1,2], Jiaqiang Yan[3,4], Craig A. Bridges[6], Andrei T. Savici[2,7], Bryan C. Chakoumakos[1,2], Mark D. Lumsden[1,2], David Alan Tennant[1,2], Roderich Moessner[8], David G. Mandrus[3,4] and Stephen E. Nagler[1,2]

The celebrated Kitaev quantum spin liquid (QSL) is the paradigmatic example of a topological magnet with emergent excitations in the form of Majorana Fermions and gauge fluxes. Upon breaking of time-reversal symmetry, for example in an external magnetic field, these fractionalized quasiparticles acquire non-Abelian exchange statistics, an important ingredient for topologically protected quantum computing. Consequently, there has been enormous interest in exploring possible material realizations of Kitaev physics and several candidate materials have been put forward, recently including α-$RuCl_3$. In the absence of a magnetic field this material orders at a finite temperature and exhibits low-energy spin wave excitations. However, at moderate energies, the spectrum is unconventional and the response shows evidence for fractional excitations. Here we use time-of-flight inelastic neutron scattering to show that the application of a sufficiently large magnetic field in the honeycomb plane suppresses the magnetic order and the spin waves, leaving a gapped continuum spectrum of magnetic excitations. Our comparisons of the scattering to the available calculations for a Kitaev QSL show that they are consistent with the magnetic field induced QSL phase.

npj Quantum Materials (2018)3:8 ; doi:10.1038/s41535-018-0079-2

INTRODUCTION

The exactly soluble Kitaev model consists of $S = ½$ spins on the honeycomb lattice interacting with anisotropic ising interactions along the three symmetry inequivalent bonds.[1] The insight that Kitaev physics might be realized in practice[2] has stimulated investigations of candidate materials, recently including α-$RuCl_3$.[3–16] In all the systems studied to date significant non-Kitaev interactions induce magnetic order at low temperature.[3,17,18] However, in-plane magnetic fields of roughly 8 T suppress the long-range magnetic order in α-$RuCl_3$,[3–10] raising the intriguing possibility of a field-induced quantum spin liquid (QSL)[11] exhibiting non-Abelian quasiparticle excitations. Here we present inelastic neutron scattering (INS) in α-$RuCl_3$ in an applied magnetic field.

The insulating magnetic material α-$RuCl_3$ is comprised of van der Waals coupled honeycomb layers of $4d^5$ Ru^{3+} cations nearly centered in edge-sharing $RuCl_6$ octahedra. A strong cubic crystal field combined with spin-orbit coupling leads to a Kramer's doublet, nearly perfect $J = ½$ ground state,[12,15,16] thus satisfying the conditions necessary for producing Kitaev couplings in the low energy Hamiltonian.[2] Similar to the widely studied honeycomb[17] and hyperhoneycomb[18] Iridates, at low temperatures α-$RuCl_3$ exhibits small-moment antiferromagnetic (AFM) zigzag order[4,14,19,27] with $T_N \approx 7$ K for crystals with minimal stacking faults. In the zigzag state the magnetic excitation spectrum shows well-defined low-energy spin waves with minima at the M-points (See Supplementary Fig. S1 in Supplementary Materials (SM) for the Brillouin Zone (BZ) definition) as well as a broad continuum that extends to much higher energies centered at the Γ points.[12–14] Above T_N the spin waves disappear but the continuum remains, essentially unchanged until high temperatures of the order of 100 K.[12–14] In analogy with the situation for coupled spin- ½ AFM Heisenberg chains,[20] the high energy part of the continuum has been interpreted as a signature of fractionalized excitations.[12–14] The overall features of the INS response resemble those of the Kitaev QSL[21–23] and are consistent with an unusual response seen in Raman scattering,[22–25] suggesting that the system is proximate to a QSL state exhibiting magnetic Majorana fermion excitations.[13,14] It is thus of great interest to investigate the nature of the excitations in the field-induced disordered state.[3–11] We show that at a field of 8 T, the spin waves characteristic of the ordered state vanish throughout the BZ. The remaining single dominant feature of the response is a broad continuum centered at the Γ point, signature of fractionalized excitations.[12–14] This provides compelling evidence that a field-induced QSL state has been achieved.

RESULTS

To investigate this phenomenon, high-quality single crystals of α-$RuCl_3$ were grown using vapor-transport techniques.[14,19] Figure 1 shows bulk susceptibility and neutron diffraction measurements, demonstrating the suppression of the zigzag order (Fig. 1a) when

[1]Quantum Condensed Matter Division, Oak Ridge National Laboratory, Oak Ridge, TN 37831, USA; [2]Neutron Scattering Division, Oak Ridge National Laboratory, Oak Ridge, TN 37831, USA; [3]Materials Science and Technology Division, Oak Ridge National Laboratory, Oak Ridge, TN 37831, USA; [4]Department of Materials Science and Engineering, University of Tennessee, Knoxville, TN 37996, USA; [5]Department of Physics, Cavendish Laboratory, JJ Thomson Avenue, Cambridge CB3 0HE, UK; [6]Chemical Sciences Division, Oak Ridge National Laboratory, Oak Ridge, TN 37831, USA; [7]Neutron Data Analysis and Visualization Division, Oak Ridge National Laboratory, Oak Ridge, TN 37831, USA and [8]Max Planck Institute for the Physics of Complex Systems, Dresden D-01187, Germany
Correspondence: Arnab Banerjee (arnabanerjee@gmail.com) or Paula Lampen-Kelley (kelleypj@ornl.gov) or Stephen E. Nagler (naglerse@ornl.gov)
Arnab Banerjee and Paula Lampen-Kelley contributed equally to this work.

Received: 16 July 2017 Revised: 21 December 2017 Accepted: 8 January 2018
Published online: 20 February 2018

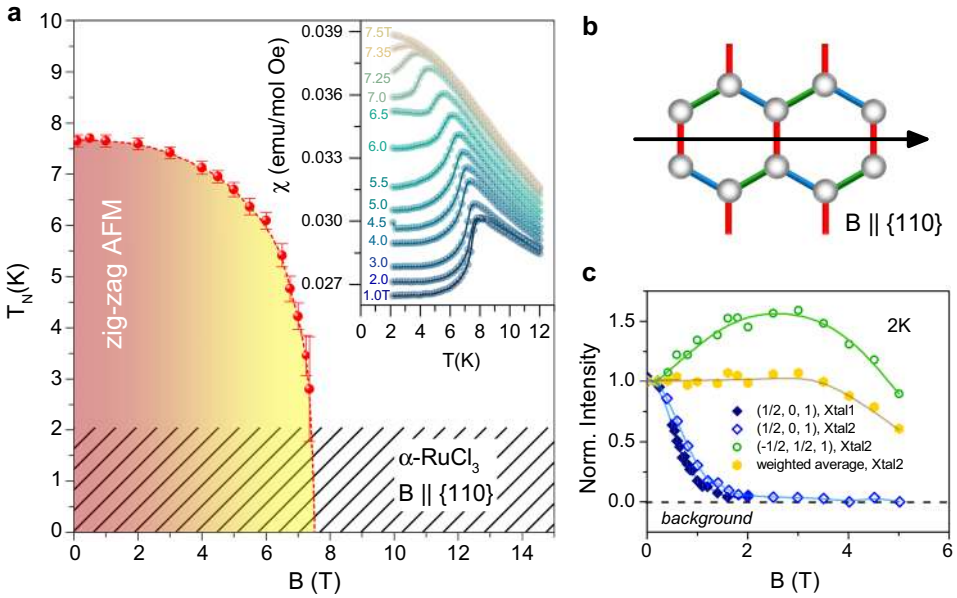

Fig. 1 Field-evolution of the zigzag order in α-$RuCl_3$: Bulk susceptibility and diffraction are shown as a function of magnetic field **b** applied along a reciprocal {110} direction. Note that the {110} is equivalently one of (1, 1, 0), (−1, 2, 0) or (2, −1, 0) directions. **a** Néel temperature vs. **b** determined from the local maximum in temperature-dependent magnetic susceptibility curves measured in fixed fields (i.e., where $d\chi/dB = 0$) Error bars are determined from the FWHM of a Gaussian fit to the peak in the derivative $d^2\chi/dB^2$ at the local maximum point (inset). For each field, χ (T) was collected on warming after cooling in zero magnetic field. The region below the experimental base temperature is indicated by hash marks. **b** Schematic of the magnetic field direction in the honeycomb plane. **c** Magnetic Bragg peak intensity normalized to the zero-field value (i.e., I(B)/I(B = 0)). The field is applied in the (−1, 2, 0) direction perpendicular to the (H, 0, L) plane. Blue diamonds show the suppression of the in-plane (1/2, 0, 1) magnetic peaks in two different crystals, 'Xtal1' and 'Xtal2', measured at HYSPEC (solid symbols) and CORELLI (open symbols). The green circles show the out-of-plane magnetic peak at (−1/2, 1/2, 1) measured at CORELLI (See Methods for instrument parameters). The yellow symbols represent the weighted average intensity over magnetic peaks with L = 1. In this average, the peaks within the (*H*, 0, *L*) plane contribute 1/3 of the intensity. Solid lines are a guide to the eye. Error bars represent one standard deviation assuming Poisson counting statistics

the field is applied along the ζ = (−1, 2, 0) (trigonal notation, see e.g., refs.[14,19,26]) or equivalent directions (Fig. 1b). The local maximum in the susceptibility, where $d\chi/dB = 0$, occurs at $T_N = 7.5$ K at 0.1 T, close to the location of the zero-field heat capacity anomaly in single-phase $RuCl_3$ crystals with ABC magnetic stacking.[19] With increasing field, T_N shifts to lower temperatures and the transition is not observed beyond $B_C = 7.3$ (3) T.

Magnetic Bragg peaks associated with the zigzag spin order appear below T_N at (½, 0, L), (0, ½, L) and (½, −½, *L*) where $L \neq 3n$.[10,14,19,26,27] Consistent with Sears et al.,[10] magnetic fields of 2 T along {110}-equivalent directions completely suppress the intensity of magnetic Bragg peaks with **Q** ⊥ **B** as seen in Fig. 1c. Conversely, peaks with a significant projection of **Q** along **B** gain intensity at low fields with increasing fields (Supplementary Fig. S2). This intensity redistribution can signify a reorientation of the ordered moments to lie perpendicular to the field direction or a depopulation of domains with moments aligned along the field direction.[10] The weighted average intensity of magnetic peaks with $L = 1$ is roughly flat up to $B \approx 3.5$ T and then follows a downward trend. (Supplementary Fig. S3 shows additional details for the peaks at (½, 0, 1) as well as (½, 0, 2)).

Figure 2 shows time-of-flight INS from a 740 mg single crystal mounted with the (H, 0, L) scattering plane horizontal, and a vertical magnetic field applied in the ζ = (−1, 2, 0) direction (see Methods section). The scattering at 2 K in zero field (Fig. 2a) shows low-energy, gapped spin waves with the expected minima at the (±1/2, 0, *L*) M points. The spin waves also show local minima at the Γ ($H = 0$) and Y ($H = 1$) points. (See Supplementary Fig. S4 for constant Q-cuts at these locations). The signal near the Γ point, however, is dominated by a broad continuum extending to higher energies, consistent with previous measurements.[12–14]

Figure 2b–e, show the evolution of the spectrum at 2 K in 2 T increments from $B = 2$ to 8 T. At $B = 2$ T the spin wave intensity is increased over most of the BZ. This is consistent with expectations for the neutron scattering cross-section. A possible explanation is that at 2 T the ordered moment direction is perpendicular to the applied field, and nearly parallel to (1/2, 0, 1). For simple spin wave models, the neutron scattering cross-section shows diminished intensity of the M point magnetic Bragg peaks with **Q** ⊥ **B** and an enhanced scattering intensity for the attendant spin waves at the same wave-vectors since the latter represent fluctuations of components perpendicular to the ordered moment. The spin waves persist as the field is increased to 4 T (Fig. 2c), and begin to lose intensity by 6 T (Fig. 2d). At 8 T, above B_C, spin-wave scattering is totally suppressed and the intensity of the continuum is enhanced (Fig. 2e). The response is an intense, and apparently gapped, column of scattering at the Γ point. Over most of the range, in particular at higher energies, the 8 T spectrum bears a strong resemblance to the zero-field spectrum just above T_N (Fig. 2f).[13,14]

Further details of the in-field spectra are presented in Fig. 3 (also Figs. S4-S7). Constant-Q cuts at the M point between 0 and 6 T in Fig. 3a and S7 show a spin wave at $E = 2.25 \pm 0.11$ meV, consistent with previous zero-field experimental results.[14,28] The cuts verify that the spin-wave intensity is enhanced at 2 T, gradually reduced by 6 T, and completely absent at 8 T, consistent with the suppression of magnetic order above B_C.

Figures 3b and S5 show constant-Q cuts at the zone center (Γ point, $H = 0$). The zero-field cut at 2 K exhibits a peak at $E = 2.69 \pm 0.11$ meV, consistent with a recent observation of the zone-center magnon by THz spectroscopy.[29] The scattering is largely unchanged up to 4 T (Supplementary Fig. S5a). Conversely, at 6

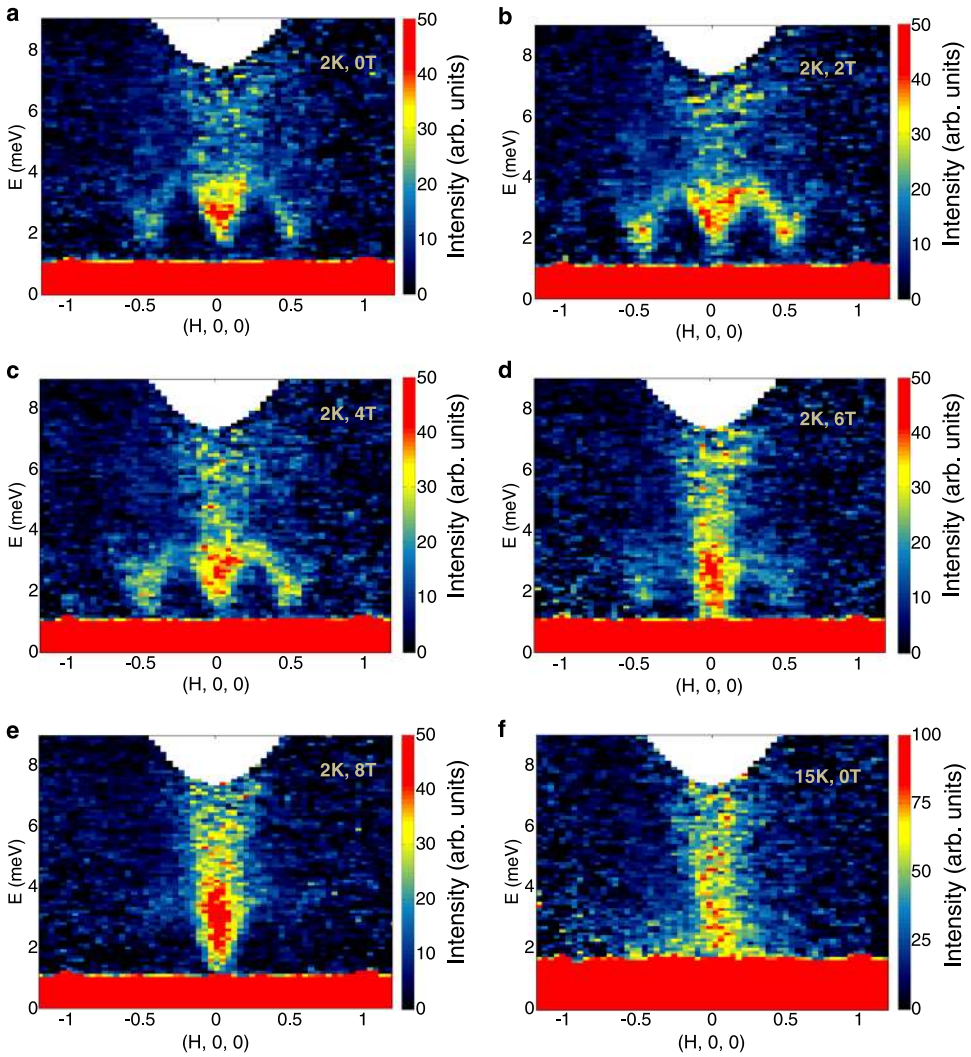

Fig. 2 Field and temperature dependence of INS along (*H*, 0, 0): Data obtained on a 740 mg single crystal α-$RuCl_3$ using the HYSPEC chopper spectrometer with Ei = 17 meV (see Methods). **a**–**e** Measurements at $T = 2$ K with an external field applied along the ζ= (−1, 2, 0) direction (perpendicular to (H, 0, 0)) using a Fermi chopper frequency of 240 Hz. The field strengths are **a** 0 T, **b** 2 T, **c** 4 T, **d** 6 T, and **e** 8 T. The slices shown are integrated over ranges $\Delta\zeta = [-0.05, 0.05]$ (in units of 2.1 $Å^{-1}$, see Supplementary Fig. S1) and $\Delta L = [-2,2]$ (in units of 0.37 $Å^{-1}$). The energy continuum at the Γ point is visible at all fields. The low-field data clearly shows the spin-wave spectrum along the (H, 0, 0) direction, with minima at the special points, Y-M-Γ-M-Y, of the 2D honeycomb BZ (see Fig. S1 for BZ definitions). **f** The zero-field spectrum at $T = 15$ K, using a Fermi chopper frequency of 120 Hz (see Methods)

T the low energy scattering has "filled-in", suggesting that the energy gap at the Γ point has closed (Fig. 3b, S5a). On further increasing the field to 8 T, the scattering consists of a broad peak centered around 3.4 meV that merges into the higher energy continuum. Extrapolation of the low-energy Γ-point spectrum to the background intensity level suggests a re-opening of a new gap by 8 T (Fig. 3b and S5b). To further elucidate the evolution of the gaps, we show the comparison of the 2 T and 6 T spectra from Fig. 3b, with the 0 T spectrum subtracted, in Fig. 3c. The extra intensity gained at low energies with increasing field to 6 T indicates the closure of the low-energy spinwave gap by 6 T. In Fig. 3d, the re-opening of the spingap at 8 T is emphasized by plotting the 8 T spectra with the 6 T spectrum subtracted, which also clearly shows a shift of the low-energy spectral weight to higher frequencies (see discussion in Supplementary Materials). While the appearance of a field-induced gap in the spectrum of spin excitations above B_C has been suggested by nuclear magnetic resonance (NMR)[9] and inferred from thermal transport[7] and specific heat[8,10] measurements, this is a direct observation of the phenomenon.

Figure 3e (also Supplementary Fig. S6) plots the wave-vector dependence of the $T = 2$ K scattering at different fields, integrated over the energy interval[5,7] meV. As seen previously,[13,14] the scattering profile is a peak centered at the Γ point. At low temperatures and low fields, the peak width is broader, reflecting contributions associated with enhanced correlations related to the zigzag order.[14] A similar comparison of the $T = 2$ K, $B = 8$ T with the $T = 15$ K, zero-field scattering in Fig. 3f demonstrates near-quantitative agreement between the two magnetically disordered states. This is true over the available data range for energy transfers above the maximum of the spin wave band.

It has been shown previously[13,14] that the energy continuum observed at the Γ point in zero field both above and below T_N is similar to the $T = 0$ response function of a Kitaev QSL,[21–23] and therefore may be a signature of fractionalized excitations associated with proximity to a QSL. Combined exact diagonalization and density matrix renormalization group (DMRG)

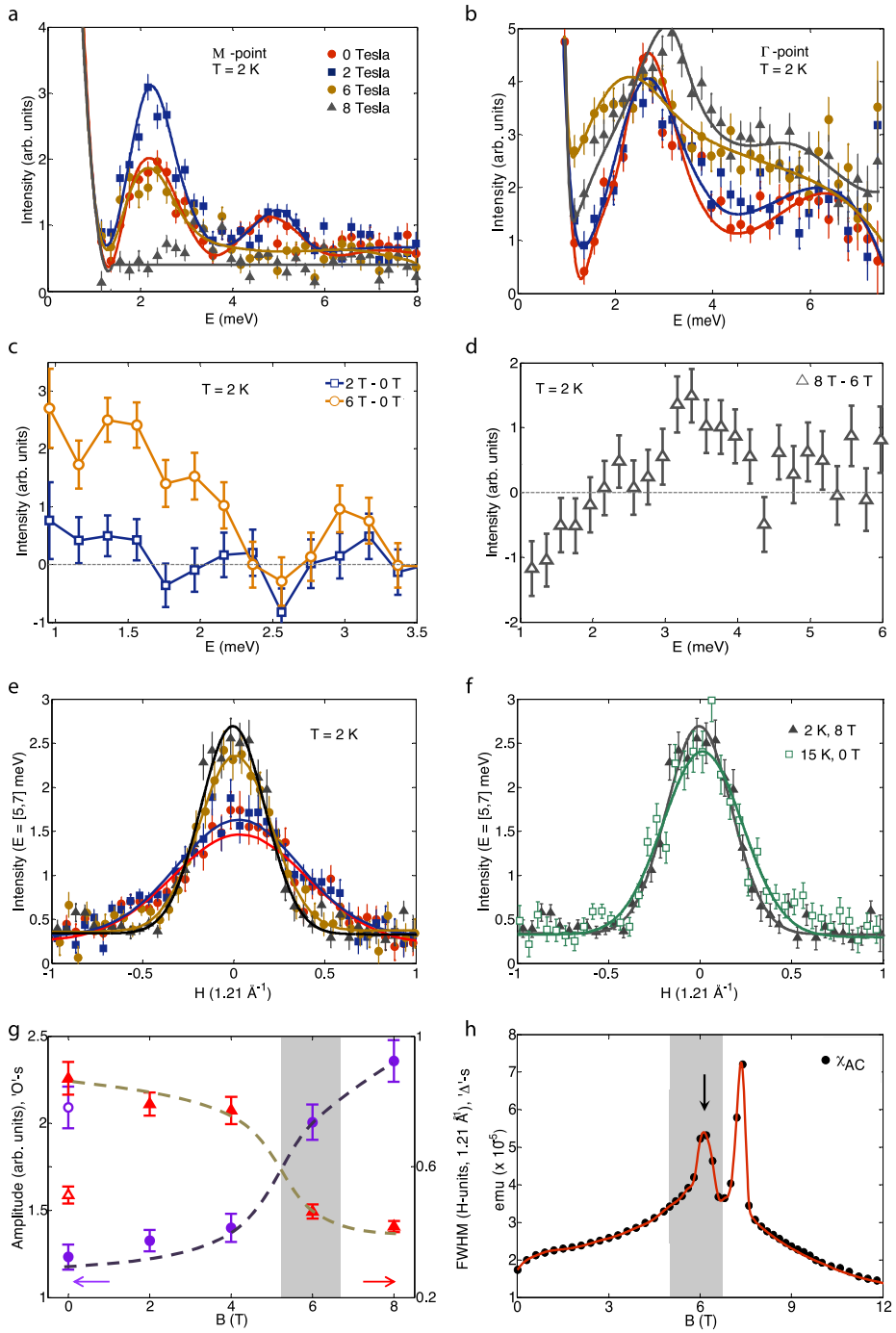

Fig. 3 Detailed field dependence of the response: The field is applied in the direction of $\zeta = (-1, 2, 0)$, and field values are defined in the legend of panel a. **a**, **b** Constant Q cuts showing the energy dependence of the scattering. The data are integrated over the wave vector ranges $\Delta H = [-0.1, 0.1]$, $\Delta\zeta = [-0.05, 0.05]$ and $\Delta L = [-2, 2]$ (See Supplementary Fig. S1 for units). Lines are guides to the eye. **a** Scattering at the M point (1/2, 0, L) shows that the energy of the spin-wave peak at 2.2 ± 0.2 meV does not change with fields up to 6 T. At 8 T the spin waves are suppressed. Defining the energy gap as the point where inelastic scattering exceeds the background leads to value of at least 1.6 ± 0.2 meV. The gap at the M point is also independent of fields up to 6 T (See supplementary fig. S7). **b** Scattering at the Γ point showing the evolution of the spectrum. The lowest energy zero-field spin-wave peak occurs at 2.69 ± 0.11 meV. The energy gap for the 0–4 T spectra is 1.8 ± 0.2 meV. The gap appears closed at 6 T, but has reopened at 8 T. At 8 T the spectrum shows higher intensity for all energies above the gap. **c** The 2 T (blue) and 6 T (orange) constant Q cuts at the Γ-point (from panel **b**) is shown with the corresponding 0 T data subtracted. **d** The 8 T constant Q cuts at the Γ-point (from panel **b**) is shown with the corresponding 6 T data subtracted. (See supplementary fig. S5 for 4 T data). **e** $T = 2$ K constant energy cuts integrated over $\Delta\zeta$ and ΔL ranges as described above, and energy range $E = {}^{5,7}$ meV, showing the evolution of the peak height and width of the continuum at 0, 2, 6 and 8 T. (See supplementary fig. S6 for 4 T data). **f** The same cuts comparing the data at $T = 2$ K, 8 T (grey triangles) and $T = 15$ K, 0 T (green open squares) demonstrating an overall quantitative agreement of the intensity and width of the Γ point continuum. The 15 K data is scaled by a factor of 2 to account for using a different chopper frequency (see Methods). In (**c**) and (**d**) the solid lines are least-square fits to a Gaussian peak plus a constant background. **g** The peak height (circles) and FWHM (triangles) of the continuum as a function of field at $T = 2$ K (solid symbols) and $T = 15$ K (open symbols). The field dependence hints at a discontinuous jump close to 6 T (crossover region, shaded.) Lines are guides to the eye. **h** AC susceptibility (Re(χ_{AC}))measured at $T = 2$ K with a frequency of 1 kHz shows two anomalies at $B_{C1} = 6.1 \pm 0.5$ T and $B_{C2} = 7.3 \pm 0.3$ T. In all panels (**a**–**g**) the error bars represent one standard deviation assuming Poisson counting statistics

calculations[11] for extended Kitaev-Heisenberg Hamiltonians have provided indications for a magnetic field-induced transition from zigzag order to a gapped QSL state. Our neutron scattering results are overall consistent with the interpretation of NMR experiments by Baek et al.[9] The disappearance of spin waves at B_C, combined with the appearance of a new gap in the high-field continuum excitation spectrum unconnected with spin waves, provides significant evidence for an interesting field-induced QSL in α-$RuCl_3$.

DISCUSSION

The removal of magnetic long-range order by the field enables comparing the measured energy-dependent scattering to a QSL-based theory over a large portion of the bandwidth of the magnetic excitations. The full effective magnetic Hamiltonian describing α-$RuCl_3$ has not been definitively determined so that the concomitant dynamic response functions remain unknown. In view of this, as a starting point, it is reasonable to compare the results to exact calculations for a Kitaev QSL. Previous such comparisons[12,14] of the zero-field measurements were restricted to high-energy features with relatively small spectral weight. The expected scattering is broad in energy for both ferromagnetic (FM) and AFM Kitaev QSLs, however in zero field the momentum dependence of the scattering was seen to be similar to the response calculated for an AFM Kitaev QSL at $T = 0$. Newly available extensions of the QSL based calculations to nonzero T[23] (see Supplementary Discussion, section D: "Theory of the *in-field* dynamical response of the Kitaev QSL" in SM) provide a theory for the full energy dependence of the scattering intensity at the Γ point. Comparing this theory to the data at 8 T reveals that the constant Q response at the Γ-point is closer to that calculated for a FM Kitaev model in an effective magnetic field (see discussion in SM, and Supplementary Figs. S8 & S9). The latter exhibits the following features that are qualitatively consistent with experiment: For temperatures comparable to, or larger than, the flux gap, the signal near $\mathbf{Q} = 0$ is a broad continuum, exhibiting only a moderately intense peak at the lower-energy threshold. Secondly, the high-frequency part of the spectrum is resilient as a function of temperature (up to $T \sim J_K$, the Kitaev constant) or magnetic field (below/above B_c). Finally, with field, the low-frequency response acquires a low-energy gap with an intensity enhanced at higher energies, similar to the Γ point continuum scattering seen in α-$RuCl_3$ above B_c (Figs. 3b, 3d, S5c and S8). This fits with the idea that the field-induced QSL evolves from the zero-field Kitaev QSL as time-reversal symmetry breaking opens a gap in the Majorana spectrum and a Majorana flux bound state (broadened by the presence of thermally excited fluxes at nonzero temperature) enhances the low-frequency response.

Despite possible differences at low energies, the overall similarity between the excitation spectra for $T > T_N$ ($B = 0$ T) and $B > B_C$ ($T = 2$ K) is quite remarkable (see Fig. 2e,f and Fig. 3f), and suggests the possibility of a simple connection between the high-energy excited states in the two regions of parameter space. Generally (see e.g., ref. [30]) one would expect Zeeman splitting to drive a softening of the gapped spin wave mode at the zigzag ordering wavevector (M-point) as the applied field is increased, eventually driving the system to a phase transition when the gap is closed at the ordering wave vector. Here the lack of any observed splitting or an M-point gap softening, coupled with the apparent softening of the gap at the Γ point, is surprising, and suggests the possibility of another field-induced transition between the zigzag state and the QSL seen above B_C. Figure 3g shows a plot of the intensity and FWHM of the scattering continuum as a function of field. The results suggest an anomaly or discontinuity within the shaded region, in the vicinity of 6 T. Further evidence is provided by the isothermal ($T = 2$ K) AC susceptibility shown in Fig. 3h. This shows a large anomaly at B_C, with a second anomaly near 6 T. Whether or not this indicates a second transition, and thus the presence of an intermediate phase between the ordered magnet and a field-induced QSL is the subject of further investigation.

To conclude, we have shown that with a magnetic field applied in the {110} direction, long-range magnetic order in α-$RuCl_3$ disappears above a threshold field B_C. Moreover, above B_c the high-frequency spectrum of magnetic excitations is a broad continuum with a response function resembling that expected for a Kitaev QSL. Although the width of the response in energy is similar for AF or FM Kitaev models, when the calculation includes the effects of non-zero temperature and field the distribution of spectral weight in α-$RuCl_3$ is closer to that expected for a FM model. Our data shows that some aspects of the field dependence of the response functions resemble pure Kitaev model calculations, and above B_c, the response at moderate energies is similar to the zero field response above T_N. It remains to be answered whether, and how, the field-induced gapped QSL observed in α-$RuCl_3$ is topologically distinct from the Kitaev QSL with or without broken time reversal symmetry [ref. [1], also see discussion in Supplementary Materials, section D]. The next challenge is to identify and explore its most compelling experimental signatures. This also includes more specific identification of the experimental signatures of the possible non-Kitaev terms[8,12,13,31–35] on the field induced QSL, with the aim of understanding whether it is possible to realize topologically protected edge states and quasiparticle excitations with non-Abelian statistics,[1,36] which have generated much enthusiasm in the context of topological quantum computation.[36–38]

METHODS

Synthesis and bulk characterization

Single crystals of α-$RuCl_3$ were prepared using vapor-transport techniques from pure α-$RuCl_3$ powder as described previously.[14] Crystals grown by the same method have been extensively characterized via bulk and neutron scattering techniques.[14,19] All samples measured in the current work exhibit a single magnetic phase at low temperature with a transition temperature Tc ~ 7 K, indicating high crystal quality with minimal stacking faults.[19] DC magnetization and AC susceptibility in 12 and 17 mg single crystals, respectively, were collected in DC fields of up to 14 T in a Quantum Design Physical Property Measurement System (PPMS). The magnetic field was applied along the reciprocal {110} directions as identified by Laue diffraction as described in Fig. 1b.

Neutron diffraction experiments

Elastic neutron studies in a 5 T vertical-field cryomagnet were performed at Spallation Neutron Source (SNS), Oak Ridge National Laboratory (ORNL), using the CORELLI beamline.[39] CORELLI is a time-of-fight instrument where a pseudo-statistical chopper separates the elastic contribution. A 125 mg α-$RuCl_3$ crystal was mounted on an Al plate and aligned with the (H, 0, L) plane horizontal and B along the $\zeta = (-1, 2, 0)$ vertical direction (See Fig. 1b). The crystal was rotated through 170 degrees in 2° steps. Perpendicular coverage of ±8° (limited by the magnet vertical opening) allowed access to the set of magnetic Bragg peaks of the zigzag ordered phase at the M-points within the first BZ—at (±½, 0, L) in the (H, 0, L) plane and (±½, ∓½, L) and (0, ±½, L) out of the (H, 0, L) plane with $L = \pm 1$, as well as the out-of-plane peaks with $L = \pm 2$. The data were reduced using Mantid.[40] Diffraction measurements were also obtained on the same 740 mg crystal measured used in the inelastic study using the HB1A and HB3 triple axis instruments at the High Flux Isotope Reactor (HFIR). For both HFIR measurements the sample was aligned with the (H, 0, L) scattering plane horizontal and with an applied vertical field of up to 5 T. An incident energy $E_i = 14.7$ meV was used. Detailed mesh scans and order parameter measurements confirmed that the magnetic phase transition remains sharp as the field is increased from zero (Supplementary Fig. S3) and the in-plane magnetic peaks remain at the commensurate position.

Inelastic scattering experiments

Single-crystal INS measurements were carried out on a 740 mg α-$RuCl_3$ crystal in an 8 T vertical-field cryomagnet using the HYSPEC instrument at SNS.[41] The sample was aligned in the horizontal (H, 0, L) scattering plane, with the magnetic field (**B**) parallel to the vertical $\zeta = (-1, 2, 0)$ direction (See Fig. 1b). An incident energy of $E_i = 17$ meV combined with a Fermi chopper frequency of 240 Hz yielded an experimental energy resolution FWHM = 0.88 ± 0.03 meV based on a Gaussian fit on the elastic line. The zero-field data at 15 K was obtained using a Fermi chopper frequency of 120 Hz, which increases the intensity, but broadens the energy resolution, both by a factor of 2.0, as compared to 240 Hz. The momentum resolution is unaffected. The 15 K data in Fig. 3f is scaled by the factor of 2 to allow a direct comparison of the intensity with the 2 K data taken at 240 Hz. These settings provide reasonable (*Q*, *E*) coverage and resolution with which to examine the spin-wave spectrum in the (*H*, 0, 0) direction, however using $E_i = 17$ meV, the higher-energy part of the sample spectrum (i.e., above roughly 6 meV) is limited by kinematic restrictions. Data were collected in 1° steps as the sample was rotated through 200° about the vertical axis for every temperature and field condition. Empty aluminum sample holder measurements were performed under identical conditions as the sample measurements and the resultant scattering has been subtracted from all data presented in the manuscript. Reduction of the raw data was carried out using standard data reduction routines and Python codes available within Mantid software.[40]

Data availability statement

All neutron data and related Python scripts used for preparing the figures in this manuscript is available at the SNS data servers with permission from the corresponding authors of the manuscript. The bulk susceptibility data is available upon request from PK. All additional numbers used in the plots presented in this manuscript is available from the coauthors upon request.

ACKNOWLEDGEMENTS

The authors acknowledge valuable discussions with Christian Batista, Huibo Cao, Matt Stone, Feng Ye, Andrey Podelsnyak. and Matthius Vojta. J.K. and R.M. particularly thank John Chalker and Dmitri Kovrizhin for collaboration on closely related work. A. B. and P.K. thank S. Chi, O. Garlea, N. Helton, J. Werner, R. Moody and M. B. Stone for assistance with the measurement on HB-3, CORELLI and HYSPEC and G. Martin for assistance with vector-graphics. The work at ORNL's Spallation Neutron Source and the High Flux Isotope Reactor was supported by the United States Department of Energy (US-DOE), Office of Science - Basic Energy Sciences (BES), Scientific User Facilities Division, managed by UT-Battelle LLC under contract number DEAC05-00OR22725. Part of the research was supported by the US-DOE, Office of Science - BES, Materials Sciences and Engineering Division (P.K., C.A.B. and J-Q.Y.). D.M. and P.K. acknowledge support from the Gordon and Betty Moore Foundation's EPiQS Initiative through Grant GBMF4416. The work at Dresden was in part supported by DFG grant SFB 1143 (J.K. and R.M.). J.K. is supported by the Marie Curie Programme under EC Grant agreements No.703697.

AUTHOR CONTRIBUTIONS

A.B., D.A.T., P.K., B.C., D.G.M., and S.E.N. conceived the experiments; P.K. made the 740 mg single crystal for HYSPEC data while J.Y., A.B., and C.A.B. made the 125 mg single crystal for CORELLI data; P.K. and J.-Q.Y. performed the bulk and AC susceptibility measurements; P.K., A.B., A.A.A., D.P., B.C., C.B., and Y.L. performed the HB-1A, HB-3A and CORELLI experiments; A.B., B.W., P.K., C.B., M.D.L., D.A.T., and S.E.N. performed the HYSPEC experiments while A.T.S. helped in Mantid reductions; J.K. and R.M. provided theoretical inputs based on QSL calculations; A.B. and P.K. analyzed the data; A.B., P. K., J.K., and S.E.N. produced the first draft; All authors contributed to the finalization of manuscript.

ADDITIONAL INFORMATION

Supplementary information accompanies the paper on the *npj Quantum Materials* website (https://doi.org/10.1038/s41535-018-0079-2).

Competing interests: The authors declare no competing financial interests.

Publisher's note: Springer Nature remains neutral with regard to jurisdictional claims in published maps and institutional affiliations.

REFERENCES

1. Kitaev, A. Anyons in an exactly solved model and beyond. *Ann. Phys.* **321**, 2–111 (2006).
2. Jackeli, G. & Khaliullin, G. Mott Insulators in the Strong Spin-Orbit Coupling Limit: From Heisenberg to a Quantum Compass and Kitaev Models. *Phys. Rev. Lett.* **102**, 017205–017209 (2009).
3. Kubota, Y., Tanaka, H., Ono, T., Narumi, Y. & Kindo, K. Successive magnetic phase transitions in α-$RuCl_3$: XY-like frustrated magnet on the honeycomb lattice. *Phys. Rev. B* **91**, 094422–094430 (2015).
4. Johnson, R. D. et al. Monoclinic crystal structure of α–$RuCl_3$ and the zigzag antiferromagnetic ground state. *Phys. Rev. B* **92**, 235119–235130 (2015).
5. Zheng, Z. et al. Gapless spin excitations in the field-induced quantum spin liquid phase of α-$RuCl_3$. *Phys. Rev. Lett.* **119**, 227208–227213 (2017).
6. Leahy, I. A. et al. Anomalous thermal conductivity and magnetic torque response in the honeycomb magnet α-$RuCl_3$. *Phys. Rev. Lett.* **118**, 187203–187208 (2017).
7. Hentrich, R. et al. Large field-induced gap of Kitaev-Heisenberg paramagnons in α-$RuCl_3$, https://arxiv.org/abs/1703.08623 (2017).
8. Wolter, A. U. B. et al. Field-induced quantum criticality in the Kitaev system α-$RuCl_3$. *Phys. Rev. B* **96**, 041405–041409(R) (2017).
9. Baek, S.-H. et al. Observation of a field-induced quantum spin liquid in α-$RuCl_3$. *Phys. Rev. Lett.* **119**, 037201–037205 (2017).
10. Sears, J. A. et al. Phase diagram of α-$RuCl_3$ in an in-plane magnetic field. *Phys. Rev. B* **95**, 180411–180415(R) (2017).
11. Yadav, R. et al. Kitaev exchange and field-induced quantum spin-liquid states in honeycomb α-$RuCl_3$. *Sci. Rep.* **6**, 37925 (2016).
12. Banerjee, A. et al. Proximate Kitaev quantum spin liquid behavior in a honeycomb magnet. *Nat. Mat.* **15**, 733–740 (2016).
13. Do, S.-H. et al. Majorana Fermions in Kitaev Quantum Spin Liquid α-$RuCl_3$. *Nat. Phys.* **13**, 1079–1084 (2017).
14. Banerjee, A. et al. Neutron scattering in the proximate quantum spin liquid α-$RuCl_3$. *Science* **356**, 1055–1059 (2017).
15. Plumb, K. W. et al. α-$RuCl_3$: a spin-orbit assisted Mott insulator on a honeycomb lattice. *Phys. Rev. B* **90**, 041112–041116(R) (2014).
16. Agrestini, S. et al. Electronically highly cubic conditions for Ru in alpha-RuCl3. *Phys. Rev. B* **96**, 161107–161111(R) (2017).
17. Chun, S. H. et al. Direct evidence for dominant bond-directional interactions in a honeycomb lattice iridate Na_2IrO_3. *Nat. Phys.* **11**, 462–466 (2015).
18. Ruiz, A. et al. Field-induced intertwined orders in 3D Mott-Kitaev honeycomb β-Li_2IrO_3. *Nat. Comm.* **8**, 961 (2017).
19. Cao, H. B. et al. Low-temperature crystal and magnetic structure of α–$RuCl_3$. *Phys. Rev. B* **93**, 134423–134430 (2016).
20. Lake, B., Tennant, D. A., Frost, C. D. & Nagler, S. E. Quantum criticality and universal scaling of a quantum antiferromagnet. *Nat. Mat.* **4**, 329–334 (2005).
21. Knolle, J., Kovrizhin, D. L., Chalker, J. T. & Moessner, R. Dynamics of a two-dimensional quantum spin liquid: signatures of emergent majorana fermions and fluxes. *Phys. Rev. Lett.* **112**, 207203–207207 (2014).
22. Knolle, J., Kovrizhin, D. L., Chalker, J. T. & Moessner, R. Dynamics of fractionalization in quantum spin liquids. *Phys. Rev. B* **92**, 115127–115146 (2015).
23. Yoshitake, J., Nasu, J. & Motome, Y. Fractional spin fluctuations as a precursor of quantum spin liquids: majorana dynamical mean-field study for the Kitaev model. *Phys. Rev. Lett.* **117**, 157203–157208 (2016).
24. Sandilands, L. J. et al. Scattering continuum and possible fractionalized excitations in α-$RuCl_3$. *Phys. Rev. Lett.* **114**, 147201–147205 (2015).
25. Nasu, J., Knolle, J., Kovrizhin, D. L., Motome, Y. & Moessner, R. Fermionic response from fractionalization in an insulating two-dimensional magnet. *Nat. Phys.* **12**, 912–915 (2016).
26. Park, S.-Y. et al. Emergence of the Isotropic Kitaev Honeycomb Lattice with Two-dimensional Ising Universality in α-$RuCl_3$, https://arxiv.org/abs/1609.05690 (2016).
27. Sears, J. A. et al. Magnetic order in α-$RuCl_3$: a honeycomb-lattice quantum magnet with strong spin-orbit coupling. *Phys. Rev. B* **91**, 144420–144424 (2015).
28. Ran., K. et al. Spin-wave excitations evidencing the Kitaev interaction in single crystalline α-$RuCl_3$. *Phys. Rev. Lett.* **118**, 107203–107208 (2017).
29. Little, A. et al. Antiferromagnetic resonance and terahertz conductivity in α-$RuCl_3$. *Phys. Rev. Lett.* **119**, 227201–227206 (2017).
30. Yosida, K. 'Theory of Magnetism', Springer Series in Solid-State Sciences, Vol. 122, Chapter 9.2, Springer publishing group (1998).
31. Gholke, M., Verresen, R., Moessner, R. & Pollmann, F. Dynamics of the Kitaev-Heisenberg Model. *Phys. Rev. Lett.* **119**, 157203–157208 (2017).
32. Samarakoon, A. et al. Comprehensive study of the dynamics of a classical Kitaev spin liquid. *Phys. Rev. B* **96**, 134408–134419 (2017).
33. Song., X.-Y., You, Y.-Z. & Balents, L. Low-energy spin dynamics of the honeycomb spin liquid beyond the Kitaev limit. *Phys. Rev. Lett.* **117**, 037209–037214 (2016).
34. Gohlke, M., Wachtel, G., Yamaji, Y., Pollmann, F. & Kim, Y.-B. Signatures of quantum spin liquid in Kitaev-like frustrated magnets, https://arxiv.org/abs/1706.09908 (2017).

35. Winter, S. M., Riedl, K., Kaib, D., Coldea, R. & Valenti, R. Probing α-RuCl3 beyond magnetic order: effects of temperature and magnetic field, https://journals.aps.org/prl/accepted/3f071Y60Uc11455127498f39514cf36f72492603d (2017).
36. Kitaev, A. Y. Fault-tolerant quantum computation by anyons. *Ann. Phys.* **303**, 2–30 (2003).
37. Nayak, C., Simon, S. H., Stern, A., Freedman, M. & Sharma, S. D. Non-Abelian anyons and topological quantum computation. *Rev. Mod. Phys.* **80**, 1083–1159 (2008).
38. Lahtinen, V. T. & Pachos, J. K. A short introduction to topological quantum computation. *SciPost Phys.* **3**, 021 (2017).
39. Rosenkranz, S. & Osborn, R. Corelli: efficient single crystal diffraction with elastic discrimination. *PRAMANA- J. Phys.* **71**, 705–711 (2008).
40. Arnold, O. et al. Mantid—Data analysis and visualization package for neutron scattering and μSR experiments. *Nucl. Instrum. Methods Phys. Res. Sect. A* **764**, 156–166 (2014).
41. Winn, B. et al. Recent progress on HYSPEC, and its polarization analysis capabilities. *EPJ Web Conf.* **83**, 03017 (2015).